

PNNL-33620

Resolving Lipid Structures for Threat- Agnostic Signatures

October 2022

Brooke LD Kaiser
Jennifer E Kyle

DISCLAIMER

This report was prepared as an account of work sponsored by an agency of the United States Government. Neither the United States Government nor any agency thereof, nor Battelle Memorial Institute, nor any of their employees, **makes any warranty, express or implied, or assumes any legal liability or responsibility for the accuracy, completeness, or usefulness of any information, apparatus, product, or process disclosed, or represents that its use would not infringe privately owned rights.** Reference herein to any specific commercial product, process, or service by trade name, trademark, manufacturer, or otherwise does not necessarily constitute or imply its endorsement, recommendation, or favoring by the United States Government or any agency thereof, or Battelle Memorial Institute. The views and opinions of authors expressed herein do not necessarily state or reflect those of the United States Government or any agency thereof.

PACIFIC NORTHWEST NATIONAL LABORATORY
operated by
BATTELLE
for the
UNITED STATES DEPARTMENT OF ENERGY
under Contract DE-AC05-76RL01830

Printed in the United States of America

Available to DOE and DOE contractors from
the Office of Scientific and Technical
Information,
P.O. Box 62, Oak Ridge, TN 37831-0062
www.osti.gov
ph: (865) 576-8401
fox: (865) 576-5728
email: reports@osti.gov

Available to the public from the National Technical Information Service
5301 Shawnee Rd., Alexandria, VA 22312
ph: (800) 553-NTIS (6847)
or (703) 605-6000
email: info@ntis.gov
Online ordering: <http://www.ntis.gov>

Resolving Lipid Structures for Threat-Agnostic Signatures

October 2022

Brooke LD Kaiser
Jennifer E Kyle

Prepared for
the U.S. Department of Energy
under Contract DE-AC05-76RL01830

Pacific Northwest National Laboratory
Richland, Washington 99354

Abstract

Development of threat-agnostic biosignatures is critical for the detection of and response to biological threats that go beyond the historical list-based approach. Lipids are a class of structurally diverse biomolecules that hold great promise as relevant threat-agnostic biosignatures, yet the fundamental challenge of resolving and decoding structural differences among lipids remains an obstacle in the pursuit of signature development. Structural analysis of complex lipids remains stymied due to spectral complexity and the inability to resolve low abundance lipids. To address these challenges, we integrated ozonolysis with ion mobility mass spectrometry (IMS-MS) analysis to determine the structural information for complex lipid species and (2) reduced lipid sample complexity prior to introduction into the IMS-MS using normal phase high pressure liquid chromatography (HPLC) to enable the ozonolysis of low abundance lipids. We applied these new capabilities to define the lipid structures in antimicrobial resistant (AMR) and antimicrobial susceptible (AMS) biothreat organism *Yersinia pestis* and cells infected with Severe Acute Respiratory Syndrome coronavirus 2 (SARS-CoV-2) variants.

Summary

This project sought to develop capabilities to more completely define the structural features of complex lipids, and to apply those capabilities to biological systems to explore the use of lipids as threat-agnostic signatures of biothreats. To that end, we have accomplished the following:

- Developed the ozonolysis-ion mobility mass spectrometry (Oz-IMS) capability to identify the position of double bonds in complex lipid molecules
- Developed a normal phase high pressure liquid chromatography (NP-HPLC) platform to reduce complex lipid samples by separating lipids by subclass and allowing fractionation into subclasses for downstream analyses
 - Used calibration curves to allow abundance calculations of lipids in each subclass
- Characterized the most in-depth lipidome of *Yersinia pestis*, including an antimicrobial resistant (AMR) and antimicrobial susceptible (AMS) strain
 - Identified differences between the lipidome of AMR and AMS strains
- Defined the proteome of *Yersinia pestis* A1122 (AMS) and a complementary AMR strain
 - Identified differences between the proteome of AMR and AMS strains
- Characterized the lipidome and proteome of two cell lines infected with SARS-CoV-2 variants
 - Identified the double bond position of a subset of identified lipids, including examples of lipid isomers that varied in double bond position
- Published two papers supported by efforts from this project

Acknowledgments

This research was supported by the **National Security Mission Seed**, under the Laboratory Directed Research and Development (LDRD) Program at Pacific Northwest National Laboratory (PNNL). PNNL is a multi-program national laboratory operated for the U.S. Department of Energy (DOE) by Battelle Memorial Institute under Contract No. DE-AC05-76RL01830. Part of the research was performed using the Environmental Molecular Sciences Laboratory (EMSL), a national scientific user facility sponsored by the DOE's Office of Biological and Environmental Research and located at PNNL. PNNL is a multi-program national laboratory operated for the U.S. Department of Energy (DOE) by Battelle Memorial Institute under Contract No. DE-AC05-76RL0-1830.

Contents

Abstract.....	ii
Summary	iii
Acknowledgments.....	iv
1.0 Introduction.....	1
2.0 Method Development	3
2.1 Resolving lipid structure using ion mobility separations.....	3
2.2 Establishing ozonolysis for the structural resolution of complex lipids	3
2.3 Reducing spectral complexity using normal phase HPLC	4
3.0 Generation and processing of biological samples.....	7
3.1 Antimicrobial resistance in <i>Yersinia pestis</i>	7
3.2 Infection with SARS-CoV-2 variants.....	8
4.0 Application of NP-HPLC and Oz-IMS with Biological Models.....	9
4.1 Resolving lipid structure using ion mobility separations.....	9
4.2 Identifying the lipidome of antimicrobial resistant and antimicrobial susceptible <i>Yersinia pestis</i>	10
4.2.1 The global lipidome of <i>Y. pestis</i> A1122.....	10
4.2.2 Lipidome changes with growth phase.....	10
4.2.3 Lipidome changes with antimicrobial resistance status.....	11
4.2.4 Global cellular fatty acid profile of <i>Y. pestis</i> AMR and AMS strains.....	12
4.2.5 Using ozonolysis-IMS to elucidate differences in lipid structures	14
4.2.6 Fractionated lipidome of <i>Y. pestis</i> AMR and AMS strains	15
4.3 Identifying the proteome of antimicrobial resistant and antimicrobial susceptible <i>Yersinia pestis</i>	15
4.4 Identifying the lipidome of cells infected with SARS-CoV-2 variants.....	17
4.4.1 Lipidome of SARS-CoV-2 wildtype virus infection of HEK293T cells.....	17
4.4.2 Lipidome of SARS-CoV-2 wildtype and variants virus infection of A549 cells.....	19
5.0 References.....	22

1.0 Introduction

Lipids are abundant, structurally diverse biomolecules that are critical for cellular structure and function. They compose the membranes of all living cells and are responsible for modulating membrane permeability, influencing activity of enzymes and other proteins that reside in the membrane, and promoting cell-cell communication during immune responses (Harayama and Riezman 2018, O'Donnell, Rossjohn et al. 2018). In order to achieve this variety of functions, hundreds to thousands of diverse lipid structures are made by cells. Resolving these many structural modifications has been inherently difficult and understudied. Figure 1 shows the complexity of this challenge. A lipid of a specified mass-to-charge (m/z) ratio can be resolved to a certain degree by LC separation, yet the example in Figure 1A is a common occurrence: one m/z feature is actually a combination of multiple structural isomers that have slightly different retention times, as represented by peaks I-IV. The molecular formula along with the tandem mass spectra for this m/z feature that matches to all isomers is a phosphoethanolamine (PE) head group with two fatty acid chains that are 17 and 18 carbons each. Each chain also contains a double bond. However, tandem mass spectrometry does not define how the fatty acids differ to result in the retention time separation. Figure 1B shows the diversity of possible structures that each of those resolved isomers could represent. The current standard platform is unable to define the structural reasons that the isomers are separated in retention time, including the location of double bonds in each fatty acid chain, the orientation of the double bond (i.e. cis vs. trans), the difference in the sn position (i.e. which chain is attached to which part of the head group), the presence/position of a branch on the fatty acid chain, or the possible presence of a cyclopropane ring. While all of these structural features are important functionally for the lipid molecule (for example, bacterial incorporation of cyclopropane rings during stress conditions (Poger and Mark 2015, Jiang, Duan et al. 2019), they are complex and difficult to define.

Defining these lipid structural features, however, could be game changing. There is evidence to suggest that conserved changes in lipid content and/or structure may occur in cells that possess threat phenotypes. In a recent DTRA-sponsored effort, we investigated the protein changes that occur in antimicrobial resistant (AMR) strains of the biothreat pathogens *Yersinia pestis* and *Francisella tularensis*, the causative agents of plague and tularemia, respectively (Deatherage Kaiser, Birdsell et al. 2022). Even though these organisms are from different genera, had different genetic changes that conferred AMR, and were resistant to different antibiotics, we observed consistent changes in the expression of proteins responsible for fatty acid biosynthesis, the mechanism by which bacteria make lipid chains for membrane lipids. Higher threat bacterial strains (in this case, AMR strains) may therefore possess lipid differences that could be developed into a threat-agnostic signature, and advancing lipidomics capabilities to resolve and define structural isomers is a critical step to realizing their potential.

In addition to previous work at PNNL that suggests lipid changes may exist across AMR strains of different bacteria, several projects have demonstrated that virus infection has a strong impact on the lipidome (Kyle, Burnum-Johnson et al. 2019, Kyle 2021). AMR is a widespread health problem for which testing is time-consuming and labor intensive, and SARS-CoV-2 continues to alter into different viral strains as the pandemic becomes endemic in society. Differentiation of lipid structures in this threat (AMR) vs. non-threat (AMS) as well as high vs. low virulence and transmissibility model systems would additionally aid in the development of a lipid-based threat-agnostic biosignature.

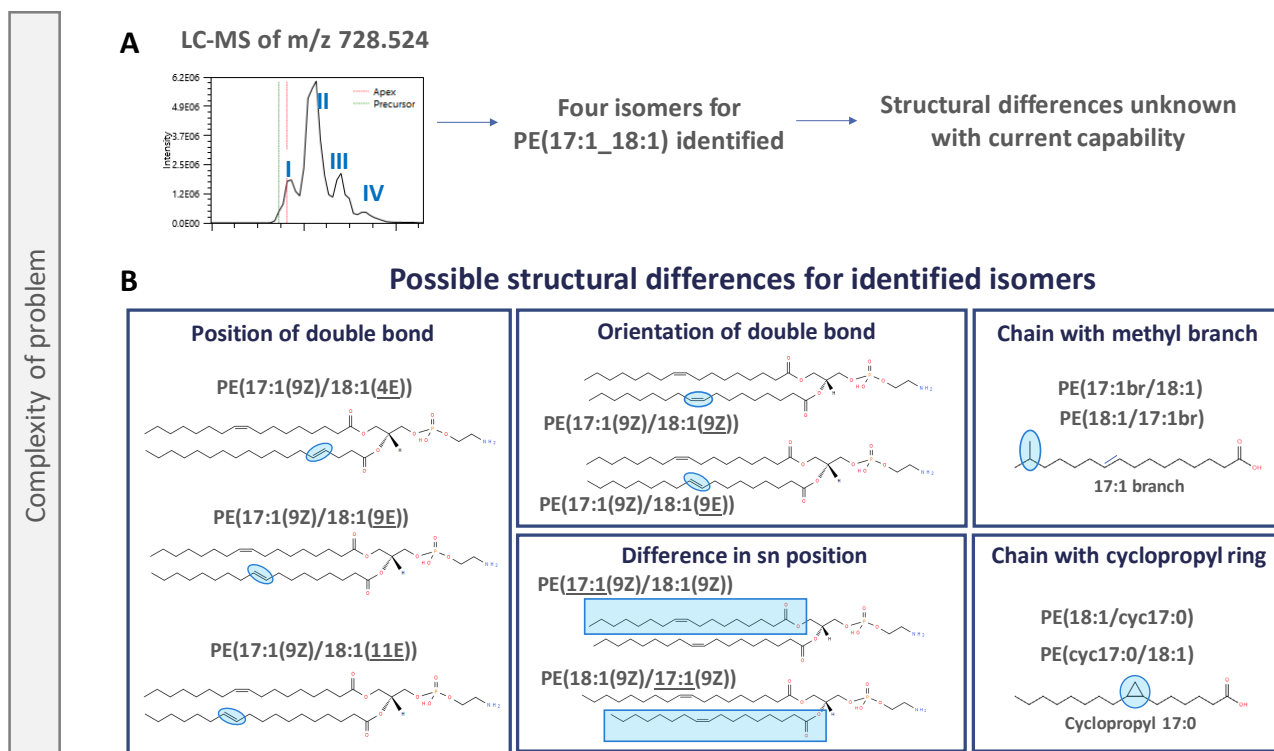


Figure 1. Resolution of lipid structural isomers is complex and challenging. (A) Our standard LC-MS/MS approach is able to identify lipids (e.g., PE(17:1_18:1)) and the presence of lipid isomers (peaks I-IV) but it is unable to distinguish the exact structural differences. (B) Potential structural features for identification of the lipid isomers identified in (A).

2.0 Method Development

2.1 Resolving lipid structure using ion mobility separations

To assess the ability of the unmodified ion mobility mass spectrometer (IMS) to resolve lipid structures, we analyzed several lipid isomer standards. The lipid standards varied in structure, focusing on similar pairs of lipids with subtle changes: (1) the position and orientation of double bond varied in fatty acid chains, (2) the chiral orientation of a fatty acid chain varied at the glycerol backbone, and (3) lipids that contain a methyl branch along the fatty acid chain. Each of the standards was analyzed on the standard lipidomics platform (LC-MS/MS), the IMS platform, and the Structures for Lossless Ion Manipulations (SLIM platform), with the exception of the lipids with varying double bond positions which were not analyzed using SLIM. Although each platform shows some success in resolving lipid structures, we are hopeful for the SLIM platform to further elucidate the structure of lipids given its success with lipid isomers unresolvable by the other two platforms.

2.2 Establishing ozonolysis for the structural resolution of complex lipids

The ozone-IMS system was adapted from Poad et al. 2018 (Poad, Zheng et al. 2018) to develop a capability for the determination of double bond position within complex lipid molecules. Ozone gas was generated from pure oxygen using the ozone generator HG-1500 (Ozone Solutions; Sioux City, IA) and introduced to the trapping region of the 6560 IMS QTOF (Agilent; Santa Clara, CA) with two modifications from (Poad, Zheng et al. 2018) (see Figure 2). The first modification was the addition of a needle valve between the destructor and the tee that connects to the ozone monitor to control the amount of ozone going to waste. Second, the PEEK line that introduces the ozone-nitrogen mixture to the trapping funnel was extended into the instrument further and directed the gas mixture directly into the path of the ions. This setup yields a concentration of about 100 g m⁻³ at an oxygen flow rate of 0.08 L min⁻¹. Also, the directed flow resulted in greater ozone reaction reproducibility from sample batch to batch. Lastly, in the modified setup, with less ozone going to the destructor, the oxygen supply lasted longer enabling hundreds of samples to be analyzed before replacement.

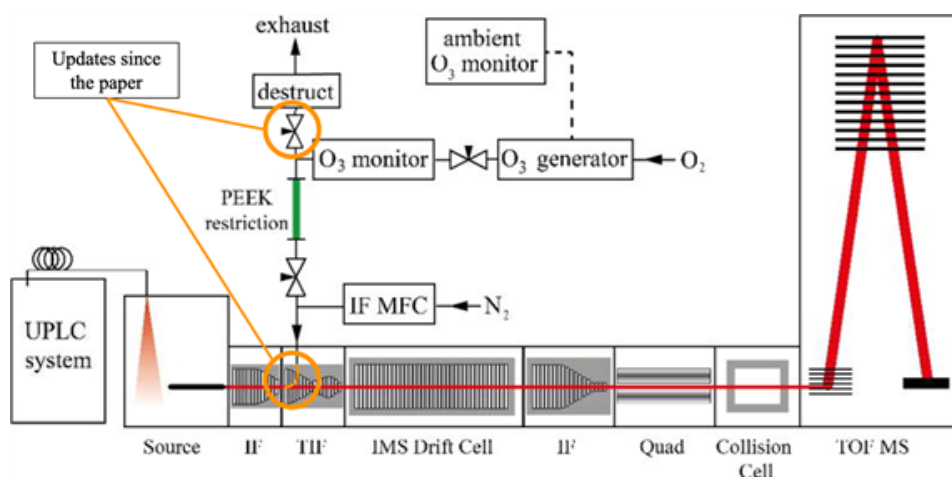


Figure 2. Schematic of ozone-IMS set up to enable ozonolysis of samples. Regions highlighted in orange are modifications from the setup previously established.

2.3 Reducing spectral complexity using normal phase HPLC

To reduce the spectral complexity of lipids to enable ozone to react with low abundance lipids, we developed a method to fractionate off line and collect lipids based on their lipid class prior to introduction to the mass spectrometer. Normal phase HPLC separates lipids based on polarity, which results in a separation of the lipids based on the subclass. Without an initial NP-HPLC separation, lipids with similar fatty acid compositions overlap when eluting from a reverse phase C18 column used in the standard lipidomics platform. The overlapping elution of similar lipids hinders the lesser abundance lipids from reacting with the ozone and subsequently prevents the identification of the double bond location.

We developed an HPLC gradient tailored to Gram-negative bacteria using standards representing the 5 dominant lipid subclasses found in these organisms, including *Y. pestis* (Figure 3). Lipid subclasses were separated using three mobile phases (Table 1) over a 38 min gradient using a YMC-PACK PVA-Sil (4.6mm x 250 mm, 5 μ m particle size) column at a flow rate of 1.0 mL/min. To evaluate the response and accuracy of the peak area for each lipid subclass, we plotted a calibration curve from 9 dilutions of each standard ranging from 20 μ g to 180 μ g on the column. A near-linear curve was obtained for all standards (Figure 4). An additional advantage of this method is the ability to determine the abundances of lipids in an entire subclass; for example, we are now able to detect whether the total amount of PE lipids is changing between conditions.

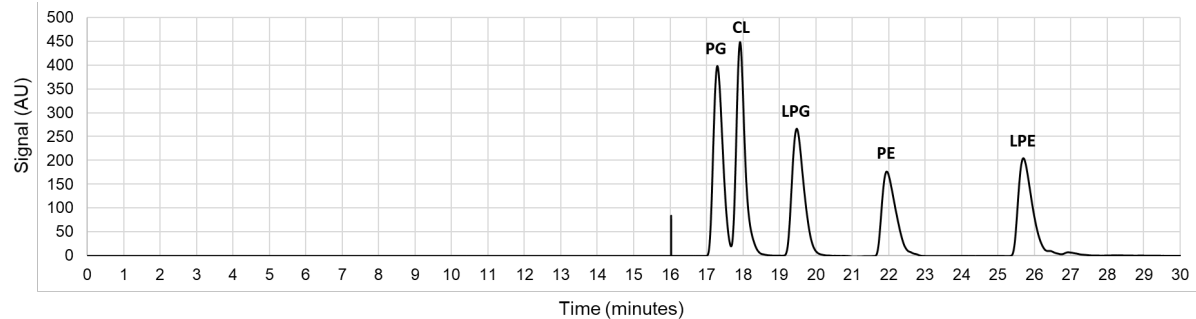


Figure 3. Gram-negative NP-HPLC profile. Chromatogram of 5 standards (180 ug on column per standard) representing the dominant types of lipids in gram-negative bacteria, including *Y. pestis*. PG = phosphatidylglycerol, CL = cardiolipin, LPG = lyso-phosphatidylglycerol, PE = phosphatidylethanolamine, LPE = lyso-phosphatidylethanolamine.

Table 1. NP-HPLC gradient

Time (min)	%A	%B	%C
0.0	100	0	0
2.0	65	35	0
10.0	50	50	0
30.0	0	50	50
30.1	0	100	0
33.0	0	100	0
33.1	100	0	0
38.0	100	0	0

%A = Hexane/Isopropanol 95/5

%B = Chloroform/Isopropanol 65/35; 0.1% triethanolamine/formic acid

%C = Methanol; 0.1% triethanolamine/formic acid

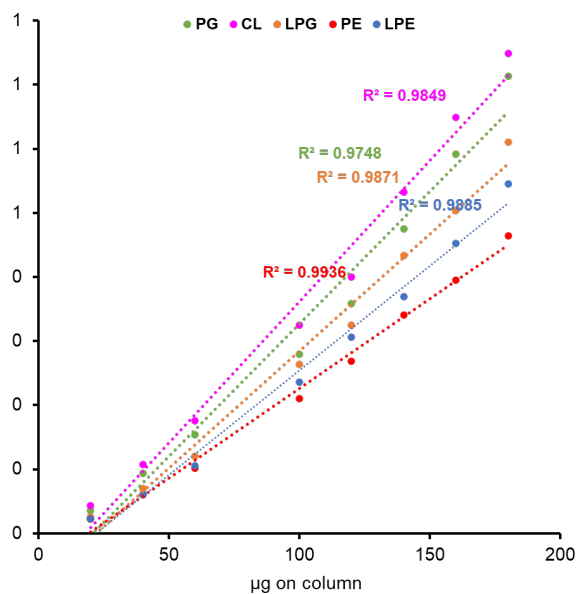


Figure 4. Calibration curve from the NP-HPLC using 5 standards. PG = phosphatidylglycerol, CL = cardiolipin, LPG = lyso- phosphatidylglycerol, PE = phosphatidylethanolamine, LPE = lyso- phosphatidylethanolamine. A near linear fit was obtained for each standard.

3.0 Generation and processing of biological samples

3.1 Antimicrobial resistance in *Yersinia pestis*

A previous study at PNNL demonstrated that significant protein changes occur in antimicrobial resistant (AMR) *Yersinia pestis*, including altered expression of proteins involved in fatty acid biosynthesis. However, lipids were not analyzed in that study. We hypothesized that there may be changes in the lipidome of AMR strains that are indicative of AMR status. To investigate this question, two strains of *Yersinia pestis* were acquired from the Wagner laboratory at Northern Arizona University via MTA for use on this project: *Y. pestis* A1122 wildtype (antimicrobial sensitive) and *Y. pestis* A1122 *rpsL* mutant (antimicrobial resistant). This *rpsL* mutant has a point mutation that renders the strain resistant to streptomycin (Andrianaivoarimanana, Wagner et al. 2022).

Our goal was to generate biomass such that we would have enough extracted lipid to split among all downstream analyses (Figure 5). To achieve this, each strain was streaked to tryptic soy agar plates (TSA plates) from frozen glycerol stocks and incubated at 37C for 48 hours. Five milliliters of tryptic soy broth (TSB) were inoculated with a single isolated colony of the appropriate strain. The three conditions that we explored were: *Y. pestis* A1122 wildtype in TSB only, *Y. pestis* A1122 *rpsL* mutant in TSB only, and *Y. pestis* A1122 *rpsL* mutant in TSB plus 64ug/uL streptomycin. Triplicate 5mL cultures of each condition were inoculated, then grown with shaking (220rpm) at 28-30C overnight.

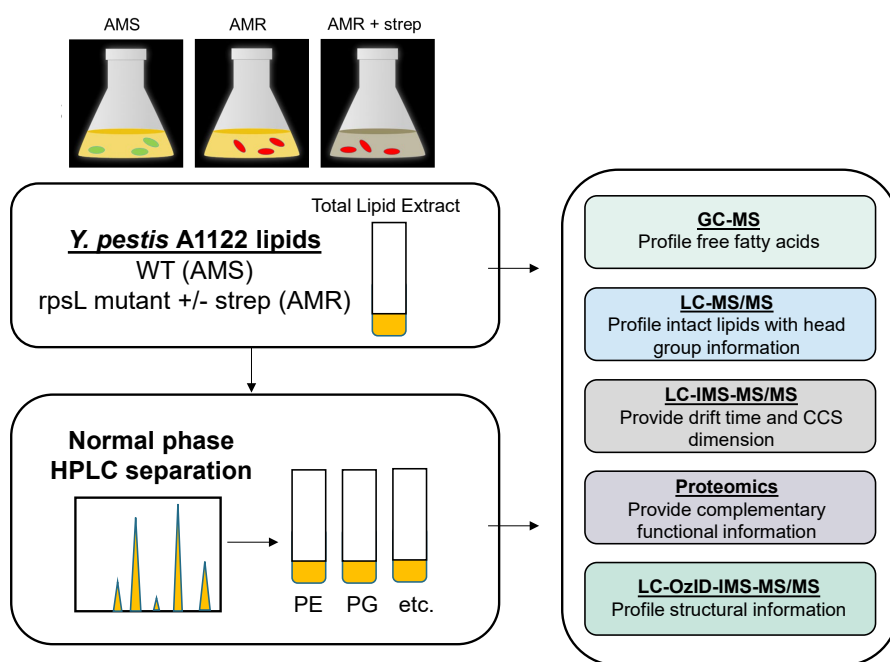


Figure 5. Overview of the experimental design to profile the lipidome of AMR and AMS *Y. pestis*.

The next day, 3mL of each culture was used to inoculate 150mL TSB (+/- streptomycin as explained above) in 500mL Erlenmeyer flasks. Cultures were grown at 28-30C with shaking

(200rpm) for either 7-8 hours (log phase cells) or 24 hours (stationary phase cells). Two growth phases were examined to attempt to capture any lipid changes that may be occurring in exponential (log) and stationary phase, as growth phase is known to influence lipid expression. The optical density at 600nm was measured for all cultures. To harvest cells, each culture was centrifuged to pellet cells and washed once with sterile phosphate buffered saline (PBS). A sample was removed following PBS washing to plate to TSA for quantification of colony forming units (CFU; bacterial concentration in the final samples). Biomass samples were then frozen at -80C prior to protein and lipid extraction via MPLEx (Burnum-Johnson, Kyle et al. 2017) and downstream analyses (Figure 5).

Extracted lipid were analyzed using LC-MS/MS as outlined in (Kyle, Crowell et al. 2017). Manually validated identifications were made using LIQUID (Kyle, Crowell et al. 2017) and MS-DIAL (Tsugawa, Ikeda et al. 2020). To obtain peak intensity values for quantification, identified lipids were aligned and gap-filled using MZmine2.0 (Pluskal, Castillo et al. 2010) and exported for statistical analysis. Extracted peptides were analyzed on a Thermo Q Exactive Orbitrap Mass spectrometer. Spectra were searched using MaxQuant against a *Y. pestis* A1122 protein database (RefSeq GCF_000222975.1).

3.2 Infection with SARS-CoV-2 variants

Two sets of experiments with the purpose to characterize the impact of infection with different SARS-CoV-2 variants on the host lipidome were conducted. Experiments were conducted with our collaborator, Fikadu Tafesse, at Oregon Health and Sciences University (OHSU) (Figure 6). In the first experiment, kidney cell line HEK293T were infected with mock-infected (n=5) and wildtype SARS-CoV-2 (n=5). Samples were collected 24 hr post-infection. In the second experiment, airway epithelial lung A549 cells were infected with wildtype and alpha, delta, and omicron SARS-CoV-2 variants (n=5 per variant). Mock infections were also collected with an n=5 per virus and all samples were collected 24 hr post-infection. Lipids and proteins were extracted in the Tafesse Lab at OHSU using approved MPLEx (Burnum-Johnson, Kyle et al. 2017) extraction and sent to PNNL for mass spectrometry analysis. Extracted lipids and proteins were analyzed as described above.

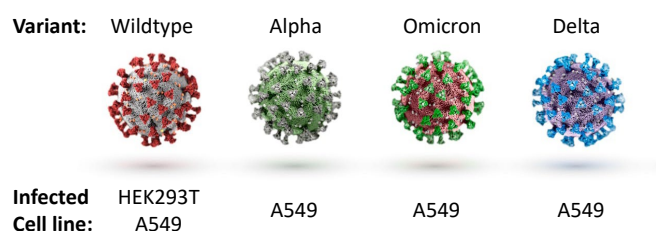


Figure 6. Overview of SARS-CoV-2 infection study design. Lipids and proteins were extracted from each infection and sent to PNNL for mass spectrometry analysis.

4.0 Application of NP-HPLC and Oz-IMS with Biological Models

4.1 Resolving lipid structure using ion mobility separations

Fatty acids with varying position of the double bond (cis 2, cis 7, and cis 9) and orientation of the double bond (cis vs. trans) were separated using liquid chromatography (LC). Using a drift tube IMS, the cis vs. trans pairs (i.e., double bond was at the same position but different orientation) had different drift times (DTs) and collisional cross sections (CCS) (Figure 7A); however, this was not observed when the orientation of the double bond remained the same (i.e., cis only) and the double bond changed position (Figure 7B). No separation was found when the chiral orientation of the fatty acid changed from S vs R along the glycerol backbone (Figure 7C). No separation was found for fatty acids containing a methyl branch at the C2 vs C3. The chiral and branched standards were also analyzed using SLIM with no separation found for the chiral lipids but separation was achieved for the branched (methyl at C2 = iso (i) and at C3 = anteiso (a)) standards (Figure 7D).

Lipid Isomer Structure	LC-MS/MS RT	LC-IMS-MS/MS DT	LC-IMS-MS/MS CCS	
A Double bond orientation				Double bond orientation
FFA 16:1 cis2	8.64	20.75	168.9	
FFA 16:1 trans2	7.91	20.91	169.4	
FFA 16:1 cis9	7.61	20.75	168.5	
FFA 16:1 trans9	7.91	20.85	169.4	
FFA 17:1 cis10	8.44	21.87	173.7	
FFA 17:1 trans10	8.84	21.35	173.0	
B Double bond position				Chiral orientation
FFA 16:1 cis2	8.64	20.75	168.9	
FFA 16:1 cis9	7.61	20.75	168.5	
FFA 16:1 cis7	7.77	20.77	168.7	
C Chiral difference				
S-PC(16:0/18:1)	20.65	37.57	294.1	
R-PC(16:0/18:1)	20.65	37.58	294.1	
S-PC(16:0/16:0)	20.45	37.04	290.0	
R-PC(16:0/16:0)	20.45	37.02	289.9	
D Methyl branch position				Branch position
16:0-a15:0 PC	20.65	37.57	294.1	
16:0-i15:0 PC	20.65	37.58	294.1	
a15:0 fatty acid	20.45	37.04	290.0	
i15:0 fatty acid	20.45	37.02	289.9	

Figure 7. Distinguishing lipid isomers using LC and drift tube IMS. Three sets of structural isomers, double bond orientation, double bond position, and chiral orientation, were assessed to determine the ability of the platforms to resolve similar but structurally distinct lipids. Example structures are provided to highlight the differences in the isomers being analyzed.

4.2 Identifying the lipidome of antimicrobial resistant and antimicrobial susceptible *Yersinia pestis*

4.2.1 The global lipidome of *Y. pestis* A1122

Using LC-MS/MS (Kyle, Crowell et al. 2017) a total of 220 unique lipid species were identified across 204 LC-MS peaks and 10 subclasses (Figure 8). More lipids were identified than LC-MS peaks given co-eluting lipids in some of the peaks and as such, all statistical results are based on 204 lipids.

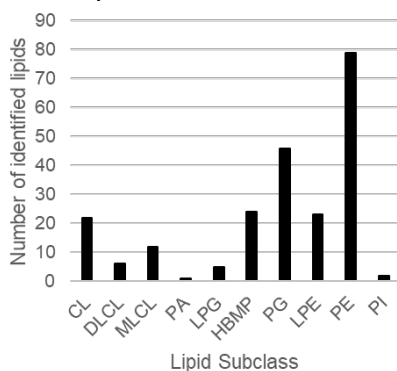


Figure 8. Distribution of identified lipids per lipid subclass in *Y. pestis* A1122. 220 lipids were identified across 10 lipid subclasses. CL = cardiolipin, DLCL = dilyso-cardiolipin, MLCL = diacyl-lyso-cardiolipin, LPG = lyso- phosphatidylglycerol, HBMP = hemibismonoacylglycerophosphate, PG = phosphatidylglycerol, LPE = lyso-phosphatidylethanolamine, PE = phosphatidylethanolamine.

4.2.2 Lipidome changes with growth phase

Growth phase had the greatest impact on the lipidome with samples clustering on a principal component analysis by growth phase (Figure 9). Of the 204 lipids identified, 163 were statistically significantly (adjusted p-value <0.05) altered between the growth phases with 85 lipids higher in log and 78 higher in the stationary phase (Figure 9 inset). Focusing on these statistically significant lipids, we conducted an enrichment analysis (Clair, Reehl et al. 2019) revealing HBMP lipids were greater and statistically enriched in the stationary phase and PE lipids were greater and statistically enriched in the log phase. We noted the lipids with the greatest fold change in the log phase contain fatty acids with 2 double bonds (8 out of 16 lipids with double bonds were in the top 10 lipids with the greatest fold change). In the stationary phase, lipids with a fold change greater than 4.5 were statistically enriched in lipids containing the fatty acid 17:1 (11 out of 14 lipids).

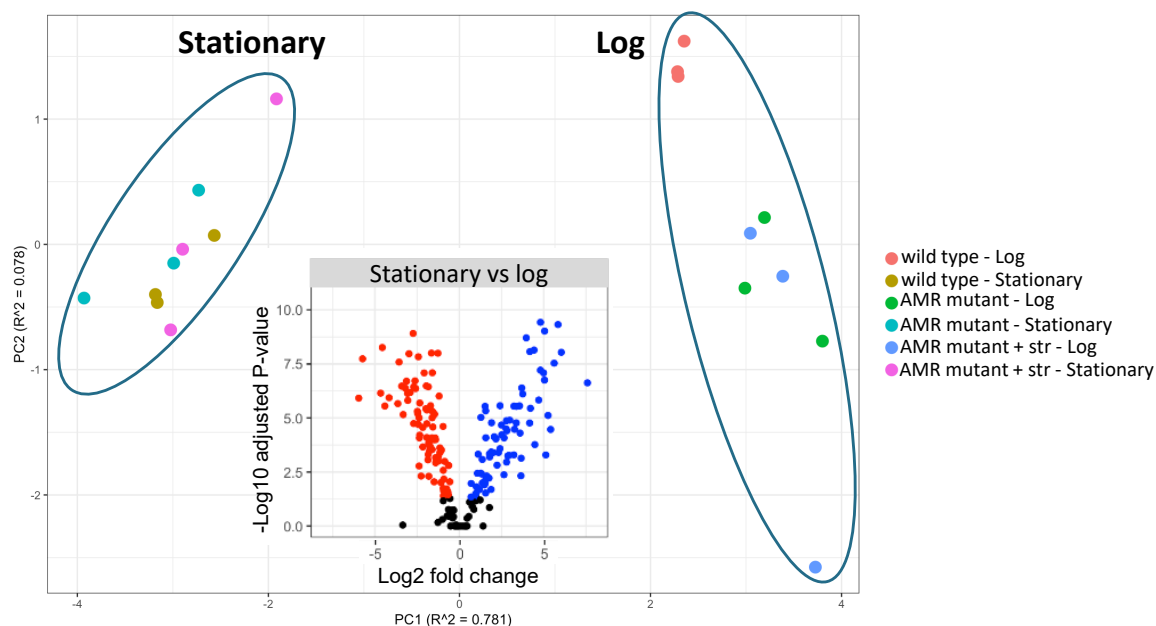


Figure 9. First two principal component scores for each condition colored by group. Stationary phase and log phase were clearly separated by PC1. Inset shows a volcano plot for stationary vs log phase based on the adjusted p-value and log₂ fold change.

4.2.3 Lipidome changes with antimicrobial resistance status

A total of 37 lipids were statistically different between AMS and AMR in the log phase (8 lipids were higher and 29 were lower in AMR mutant), and only 8 lipids were statistically different between AMS and AMR in the stationary phase (2 lipids were higher and 6 were lower in AMR mutant, Figure 10). In log phase, LPE lipids were statistically lower in the AMR mutant. The addition of streptomycin to the AMR mutant strains had little effect on the lipidome with only 2 lipids in each log and the stationary phase statistically differed.

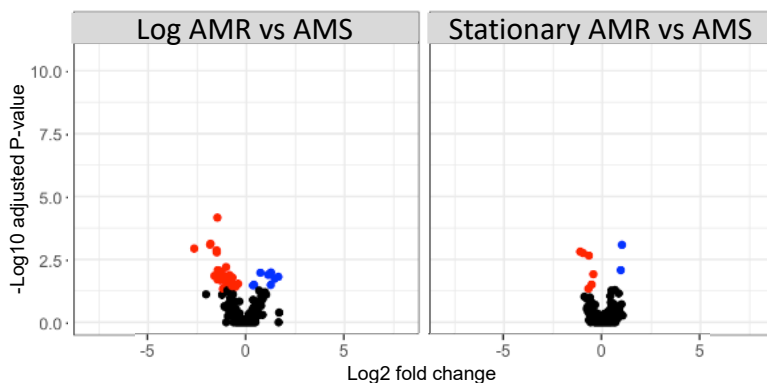


Figure 10. Volcano plot for AMR vs. AMS for log and stationary log phase based on the adjusted p-value and log₂ fold change.

4.2.4 Global cellular fatty acid profile of *Y. pestis* AMR and AMS strains

A total of 37 fatty acids were quantified in *Y. pestis*. 16 of these fatty acids were identified, including tentative or confirmed double bond positions. As with the lipidome of the complex lipids, the log and the stationary phase separated in the PCA plot (Figure 11). For both growth phases, the AMS was clustered separately from the AMR, and for log phase only the AMR and AMR plus streptomycin were slightly separated. Most of the growth phase and strain comparisons had statistically significant differences (Figure 12) including 22 of the fatty acids were found to be statistically different between at least one of the log phase conditions (Figure 13). Some of the fatty acids differed between AMS and the AMR as well as between AMR mutants. In depth stationary phase comparisons are ongoing.

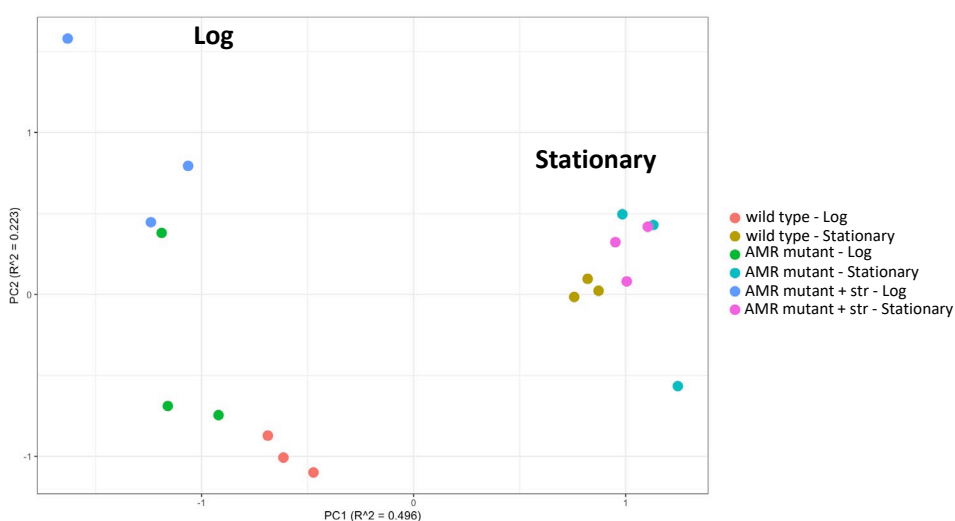


Figure 11. First two principal component scores for each condition colored by group. The stationary phase and log phase were clearly separated by PC1 with some separation of between in PC2 between the mutant and mutant plus streptomycin. Wildtype = AMS.

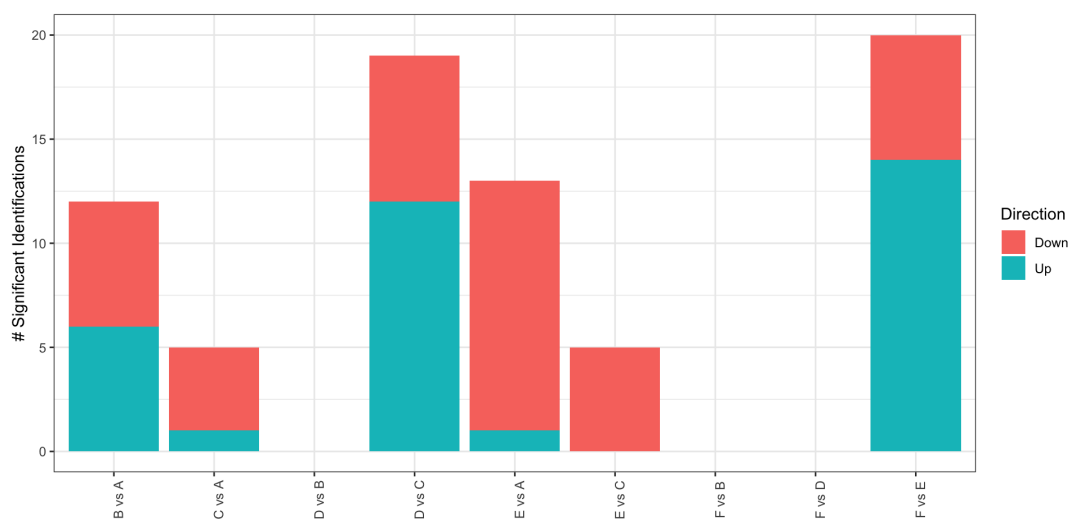


Figure 12. Number of significant identifications by statistical comparison and direction of change (based on adjusted p-values). A = wildtype – log, B = wildtype – stationary, C = AMR mutant – log, D = AMR mutant – stationary, E = AMR mutant + streptomycin – log, F = AMR mutant + streptomycin – stationary.

Fatty acid	Log2 fold change			Significance flag			Observation
	M-WT	MS-WT	MS-M	M-WT	MS-WT	MS-M	
8:0	Light Blue	Light Blue	Dark Blue	Grey	Grey	Grey	
9:0	Light Blue	Light Blue	Light Blue	Grey	Grey	Grey	
12:0	Light Blue	Light Blue	Light Blue	Grey	Grey	Grey	lower in both mutants
14:0	Light Blue	Light Blue	Light Blue	Grey	Grey	Grey	
14:1	Light Blue	Light Blue	Light Blue	Grey	Grey	Grey	lower in both mutants
14:1(11Z?)	Light Blue	Light Blue	Light Blue	Grey	Grey	Grey	
16:0	Light Blue	Light Blue	Light Blue	Grey	Grey	Grey	lower in plus strep
16:1 (13-Me,6Z?)	Light Blue	Light Blue	Light Blue	Grey	Grey	Grey	
16:1 (9Z)	Light Blue	Light Blue	Light Blue	Grey	Grey	Grey	
17:1	Light Blue	Light Blue	Light Blue	Grey	Grey	Grey	
18:0	Light Blue	Light Blue	Light Blue	Grey	Grey	Grey	lower in both mutants
18:1 (9Z)	Light Blue	Light Blue	Light Blue	Grey	Grey	Grey	
18:2 (9Z,12Z)	Light Blue	Light Blue	Light Blue	Light Blue	Light Blue	Light Blue	greater in both mutants
cyc17:0	Light Blue	Light Blue	Light Blue	Grey	Grey	Grey	
Unknown_01	Light Blue	Light Blue	Light Blue	Grey	Grey	Grey	
Unknown_03	Light Blue	Light Blue	Light Blue	Grey	Grey	Grey	
Unknown_05	Light Blue	Light Blue	Light Blue	Grey	Grey	Grey	
Unknown_06	Light Blue	Light Blue	Light Blue	Grey	Grey	Grey	
Unknown_08	Light Blue	Light Blue	Light Blue	Grey	Grey	Grey	
Unknown_09	Light Blue	Light Blue	Light Blue	Grey	Grey	Grey	lower in plus strep
Unknown_10	Light Blue	Light Blue	Light Blue	Grey	Grey	Grey	
Unknown_12	Dark Blue	Light Blue	Light Blue	Light Blue	Light Blue	Light Blue	

Figure 13. Statistically significant cellular fatty acid profile of log phase strains. Identified fatty acids that were found to be statistically significant in at least one log phase condition. As noted in the last column, some of the statistically significant fatty acids were lower in both mutants and greater in both mutants, or lower in mutant plus streptomycin (strep) only. Confirmed double bond positions are noted inside the parentheses unless there is a question mark, which signifies a tentative double bond position. M = mutant, MS = mutant plus streptomycin, WT = wildtype. Cyc17:0 = cyclopropane 17:0.

4.2.5 Using ozonolysis-IMS to elucidate differences in lipid structures

For even-chained fatty acids with only one double bond, the only confident double bond position was $n=7$ regardless of the lipid subclass. Lipids with fatty acid chains containing two double bonds indicated $n=6$ and $n=9$ were the most likely options for those lipids where an ozone reaction occurred. Lipids containing odd-chained fatty acids with the appearance of a double bond did not react with ozone; however, many even-chained lipids with one double bond position also did not react. As such it is difficult to determine if these lipids did not react due to the lack of a double bond along the chain or if the lipids were in too low abundance, or co-eluting near a more intense lipids preventing ozonolysis.

In addition to ozonolysis, we captured DT and CCS values for each lipid. Each identified subclass of lipid formed a distinct cluster and trendline when m/z vs. drift time was plotted (Figure 14A). Of the 204 lipids identified, 105 (51% of the identified lipidome) were identified as potential structural isomers of at least one other lipid. These 105 lipids fell into 42 groups of isomers where the m/z and MS/MS fragment ions are the same per isomer group but the lipids were separated by RT. Within 15 of the 42 groups, the DT and/or CCS values were distinct for at least one of the lipids in the group, meaning that the lipids within the remaining 35 isomers groups were not distinguished by DT or CCS. 7 of the 15 groups contained a PE lipid where one of the isomers has a drastically different RT (elutes approximately 5 minutes than the other lipid(s) in the group). The difference in PE lipids with a questionable RT time was further distinguished from the other PE lipids with a unique trend line (Figure 14B). A third trend line was noted in the PE lipids; however, an obvious difference resulting in the slightly shifted trend line was not identified.

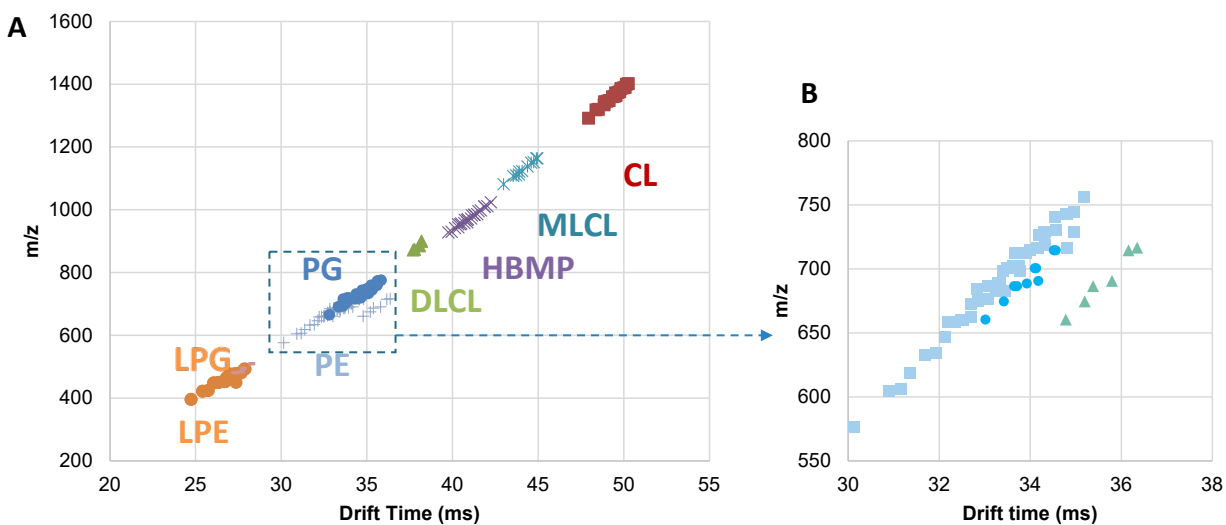


Figure 14. Trend lines of lipids identified in *Y. pestis*. A. Each identified subclass formed a distinct cluster and trend line. B. Zoomed in plot of the PE lipids, which shows three trend lines within this subclass. The blue circles do not have an obvious difference resulting in the slightly shifted trend line. The green triangles are PE lipids with questionable RTs.

4.2.6 Fractionated lipidome of *Y. pestis* AMR and AMS strains

Aliquots of the same total lipid extracts from all conditions were also analyzed by NP-HPLC, with the goal of separating complex lipid mixtures into fractions that contain lipids of only one subclass. *Y. pestis* samples were fractionated into 7 fractions (Figure 15).

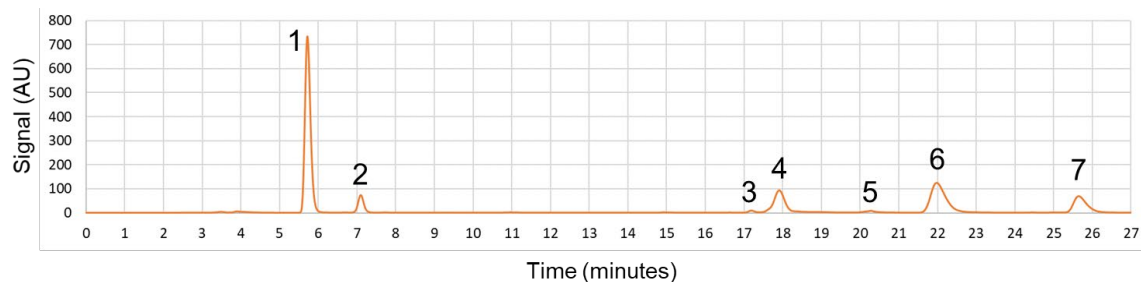


Figure 15. Normal phase HPLC profile of stationary phase *Y. pestis*. An example chromatogram of the seven peaks corresponding to different lipid subclasses that were separated and collected using normal-phase HPLC. Peak 1 = free fatty acid (FFA), peak 2 = unknown, peak 3 = phosphatidylglycerol (PG), peak 4 = cardiolipin (CL), peak 5 = lyso- phosphatidylglycerol (LPG), peak 6 = phosphatidylethanolamine (PE), peak 7 = lyso- phosphatidylethanolamine (LPE).

When the lipids identified in global and fractionated samples were compared, the largest differences were peaks associated with DLCL (dilyso-cardiolipin), MLCL (diacyl-lyso-cardiolipin), HBMP (hemibismonoacylglycerophosphate), or PI (phosphatidylinositol). These lipid species were identified in the bulk analysis, but not identified in the fractionated samples, possibly due to low abundance that precluded collection in a fraction.

4.3 Identifying the proteome of antimicrobial resistant and antimicrobial susceptible *Yersinia pestis*

A total of 1839 proteins were observed among all *Y. pestis* datasets. For each protein, we ran an analysis of variance (ANOVA) model using group as the explanatory variable. Pairwise post-hoc comparisons testing for differences in mean abundance. There were nine different comparisons of interest (Table 2). A Holm multiple test correction (Holm 1979) was used to adjust p-values for multiple comparisons. Growth phase was the most significant factor affecting protein expression, which was expected due to the changing metabolism in growth phases (Deatherage Kaiser, Birdsell et al. 2022). (Figure 16). In addition to the major changes that occur in the proteome due to growth phase, we also observed changes in the proteome based on antimicrobial resistance status (Figure 17; comparisons A vs. C, B vs. D, A vs. E, and B vs. F). Data analysis is ongoing to examine the effects of antimicrobial resistance on the *Y. pestis* proteome, including focusing on proteins suspected or known to be involved in lipid metabolism.

Table 2. Statistical comparisons of *Y. pestis* proteomics data

Nomenclature	Comparison
A vs. B	Log phase WT vs. Stationary phase WT
A vs. C	Log phase WT vs. Log phase AMR
A vs. E	Log phase WT vs. Log phase AMR-strep
B vs. D	Stationary phase WT vs. Stationary phase AMR
B vs. F	Stationary phase WT vs. Stationary phase AMR-strep
C vs. D	Log phase AMR vs. Stationary phase AMR
C vs. E	Log phase AMR vs. Log phase AMR-strep
D vs. F	Stationary phase AMR vs. Stationary phase AMR-strep
E vs. F	Log phase AMR-strep vs. Stationary phase AMR-strep

WT = wild type *Y. pestis* A1122, AMR = *Y. pestis* A1122 rpsL mutant, AMR-strep = *Y. pestis* A1122 rpsL mutant grown in streptomycin

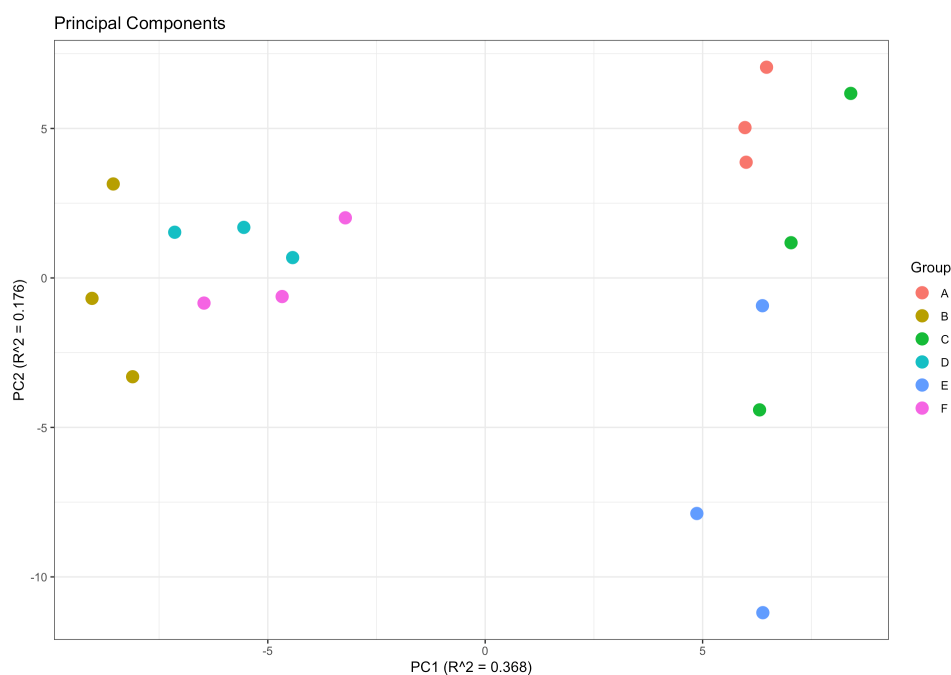


Figure 16. First two principal component scores for each *Y. pestis* sample colored by group. Note that the samples are significantly influenced by growth phase of the bacterial culture.

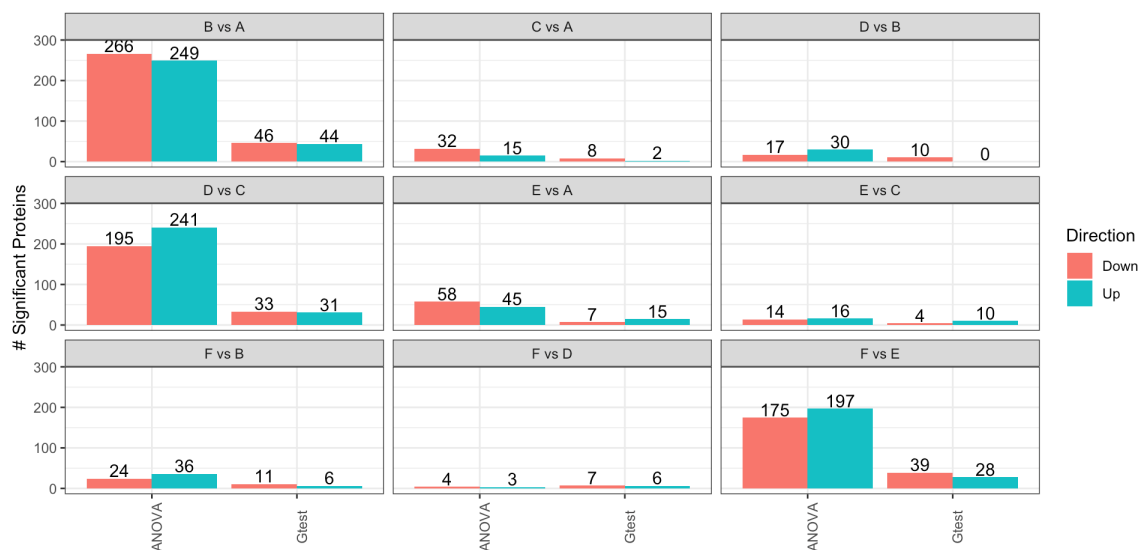


Figure 17. Number of significant *Y. pestis* proteins by statistical comparison and direction of change (based on adjusted p-values \leq 0.5).

4.4 Identifying the lipidome of cells infected with SARS-CoV-2 variants

4.4.1 Lipidome of SARS-CoV-2 wildtype virus infection of HEK293T cells

In the first experiment, kidney cells HEK293T were infected with wildtype SARS-CoV-2 and samples were collected 24 hr post infection. 514 lipids were identified with 59% significantly (adjusted p-value <0.05) altered 24hrs post-infection when compared to mock-infected cells. 26% of the lipids were identified as potential structural isomers. Interestingly, when we looked at isomer groups, we noted that 15 groups had at least one lipid isomer that was significantly altered but the other was not (Table 3). One isomer group (Group 1 in Table 3) has both lipids statistically altered but the lipids had opposing directions of change. Also, 5 of the 15 isomers groups had slightly different DT and/or CCS values. Whether this difference is structurally informative is yet to be determined. Ozone analysis was not conducted on these samples as the samples were received prior to ozone optimization.

Table 3. Lipid isomers where at least one isomer in the groups was statistically significant at 24 hr post infection.

Group #	Divergent isomer pairs	row m/z	RT	Log2FC	DT	CCS	P-value*
1	PC(0:0/18:0)_A	524.3725	8.62	-3.9	30.16	239.6	2.71E-07
	PC(0:0/18:0)_B	524.3725	9.20	1.6	30.03	238.5	2.01E-05
2	PC(15:0/16:0)_A	720.5553	19.05	-1.0	35.65	281.2	2.58E-05
	PC(15:0/16:0)_B	720.5552	19.44	-0.1	35.83	282.6	2.65E-01
3	PC(16:0/16:0)_A	734.5709	20.09	-0.7	36.22	285.6	2.89E-04
	PC(16:0/16:0)_B	734.5702	20.44	0.0	36.24	285.8	7.44E-01
4	PC(18:1/18:1)_A	786.6011	20.81	-0.7	37.2	293	1.13E-03
	PC(18:1/18:1)_B;PC(18:0/18:2)	786.6013	21.08	0.2	37.23	293.2	1.97E-01
5	PC(16:0/20:3)_B	784.5861	20.26	0.0	38.69	304.7	9.04E-01
	PC(18:1/18:2)_A	784.5859	19.34	-0.7	36.93	290.9	4.23E-04
	PC(18:1/18:2)_B;PC(16:0/20:3)_A	784.5859	19.70	0.0	37.03	291.6	8.69E-01
6	PE(18:1/18:1)_A	742.5391	21.15	-0.6	34.72	272.4	8.10E-03
	PE(18:1/18:1)_B;PE(18:0/18:2)	742.5395	21.42	-0.3	34.67	272	6.31E-02
7	PE(18:1/20:3)_A	766.5388	20.24	0.2	35.13	275.4	1.24E-01
	PE(18:1/20:3)_B	766.5394	20.85	-0.6	35.14	275.5	5.54E-04
8	PE(P-16:0/20:3)_A	724.5286	21.09	-0.4	34.49	270.7	1.36E-01
	PE(P-16:0/20:3)_B	724.5293	21.29	-0.7	34.44	270.3	5.44E-04
	PE(P-16:0/20:3)_C	724.5293	21.59	-0.9	34.49	270.7	2.44E-04
9	PE(P-16:0/20:4)_A	722.513	20.02	-1.0	34.4	270	4.04E-04
	PE(P-16:0/20:4)_B	722.5132	20.31	-0.2	34.35	269.6	1.88E-01
10	PG(18:1/18:2)_A	771.5184	14.39	-0.1	35.75	280.3	4.90E-01
	PG(18:1/18:2)_B	771.5184	14.69	-0.6	35.86	281.1	5.90E-03
11	PI(16:0/20:3)_A	859.5339	15.92	-0.3	37.24	291.4	1.49E-01
	PI(16:0/20:3)_B;PI(18:0/18:3)	859.5339	16.59	-1.1	37.36	292.3	1.88E-03
12	PI(16:1/20:4)_A	855.503	13.22	-0.9	36.91	288.9	1.10E-03
	PI(16:1/20:4)_B	855.5029	13.72	0.2	36.95	289.2	4.96E-01
13	PI(18:1/20:3)_A	885.5489	16.12	-0.4	37.98	297.1	7.93E-02
	PI(18:1/20:3)_B	885.549	16.76	-1.4	38.14	298.3	4.88E-05
14	PI(18:1/20:4)_A	883.5343	15.25	-0.4	37.7	294.9	3.66E-02
	PI(18:1/20:4)_B	883.5338	15.50	-0.1	37.8	295.7	8.26E-01
15	PI(19:0/20:4)_A	899.5641	17.73	-0.9	38.31	299.6	3.74E-03
	PI(19:0/20:4)_B	899.5641	18.15	-0.6	38.35	299.9	1.63E-01

RT = retention time

DT = drift time

CCS = collisional cross section

* = adjusted p-value

Bold text = isomer groups with slight differences in DT and/or CCS values

Enrichment analysis (Clair, Reehl et al. 2019) of the significantly increased lipids (using a p-value cutoff of <0.001) during infection revealed that lipids containing polyunsaturated fatty acids (PUFAs), in particular, those associated with triacylglycerides (TGs) and phosphatidylcholines (PCs), were statistically significantly enriched. Lipids that significantly decreased (using a p-value cutoff of <0.001) with infection were statistically enriched in monounsaturated fatty acids. Implementing an additional filtering cutoff (the lipid must also have a log2 fold change greater than 1.5), lipids that increased were also enriched in sphingolipids with a sphinganine backbone, and for lipids that decreased cardiolipins were statistically enriched.

The results from this study were complementary analyses to a larger transfection study where over 20 proteins from SARS-CoV-2 WT were isolated and transfected into HEK293T cells.

Lipidomics for each one of these transfections experiments was conducted also at PNNL. Here we showed that the results from the wildtype virus infection of the HEK293T cells aligned with some of the results from the transfection experiment enabling us to link changes in the infected lipidome to specific viral proteins. This work was published recently (Farley, Kyle et al. 2022) along with additional lipid metabolism inhibitor studies.

4.4.2 Lipidome of SARS-CoV-2 wildtype and variants virus infection of A549 cells

In this second experiment, lung epithelial A549 cells were infected with SARS-CoV-2 wildtype and 3 variants including alpha, omicron and delta. A total of 443 lipids were identified with the number of statistically significant (adjusted p-value <0.05) lipids altered compared to mock varying per virus type (Table 4). The lipidome of the different variant infections were distinct from each other and the mock infection (Figure 18). Similar to the SARS-CoV-2 wildtype HEK293T infection, 29% of the lipids were identified as potential structural isomers.

Table 4. Summary of significantly altered lipids following infection of A549 cells with different SARS-CoV-2 variants

Adjusted P-value	Alpha	Delta	Omicron	Wildtype
<0.01	124	240	151	162
<0.001	67	198	117	123

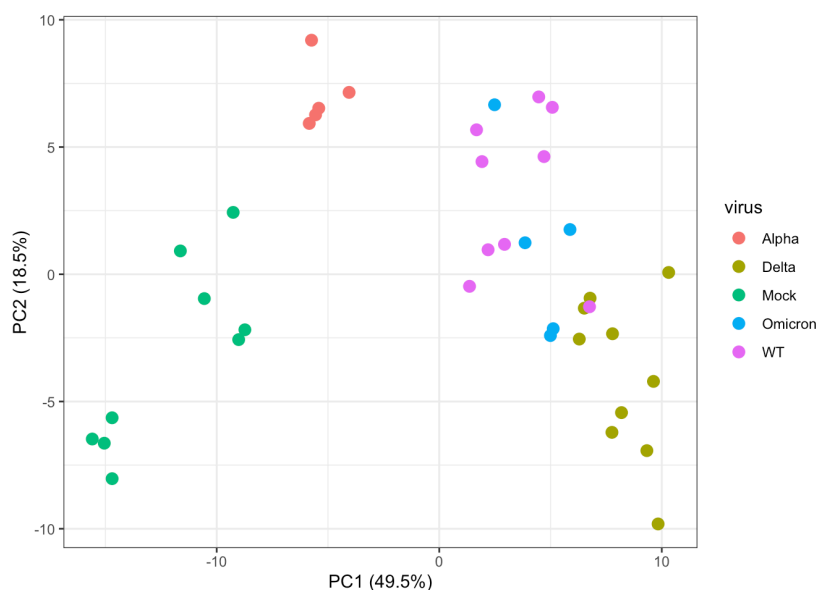


Figure 18. Principal component scores for the SARS-CoV-2 variant infection experiment in A549 cells. Mock infected cells (green) and each of the variants clustered together highlighting the differences in the lipidome at 24 hours post infection.

To resolve the structural details of the isomers, we analyzed the samples using the new ozone-IMS platform. We were able to confidently assign double bond locations to lipids in 5 isomer groups including fatty acids chains containing both monounsaturated fatty acids (i.e., 1 double bond) and PUFAs (3 plus double bonds) (Figure 19). For the first 3 isomer groups (Figure 19A), all of the statistically significant lipids are PCs and all contain the fatty acid 16:1. As shown in figure 19, the double bond positions were n=7, 9, and 10 for these lipids. N=7 is the most common position found in mammalian cells. Both the n=9 and n=7 double bonds are formed by the action of stearoyl-Coenzyme A desaturase 1 (SCD1). The n=7 position has recently been shown to be a potential marker of cardiovascular disease (Guijas, Meana et al. 2016). The other position, n=10, is most commonly found in skin and has known antimicrobial functions (Fischer, Blanchette et al. 2014). This double bond location is formed by the action of fatty acid desaturase 2 (FADS2). Proteomics analyses were conducted on these samples and will be evaluated shortly.

Two additional isomer groups and the double bond locations of the lipids were also identified. In figure 19B, both groups show that the double bond position is the same for each lipid in the group. This finding suggests that these lipids are structurally different by the sn position of the fatty acids on the glycerol unit. Previous work (Kyle, Zhang et al. 2016) has found that when structural lipid isomers are identical except for the sn position, fatty acids in the sn-2 position or fatty acids that have longer carbon chain lengths will elute before sn-1. This indicates that the B isomer in isomer groups 4 and 5 as the fatty acid or longer fatty acid chain in the sn-2 position.

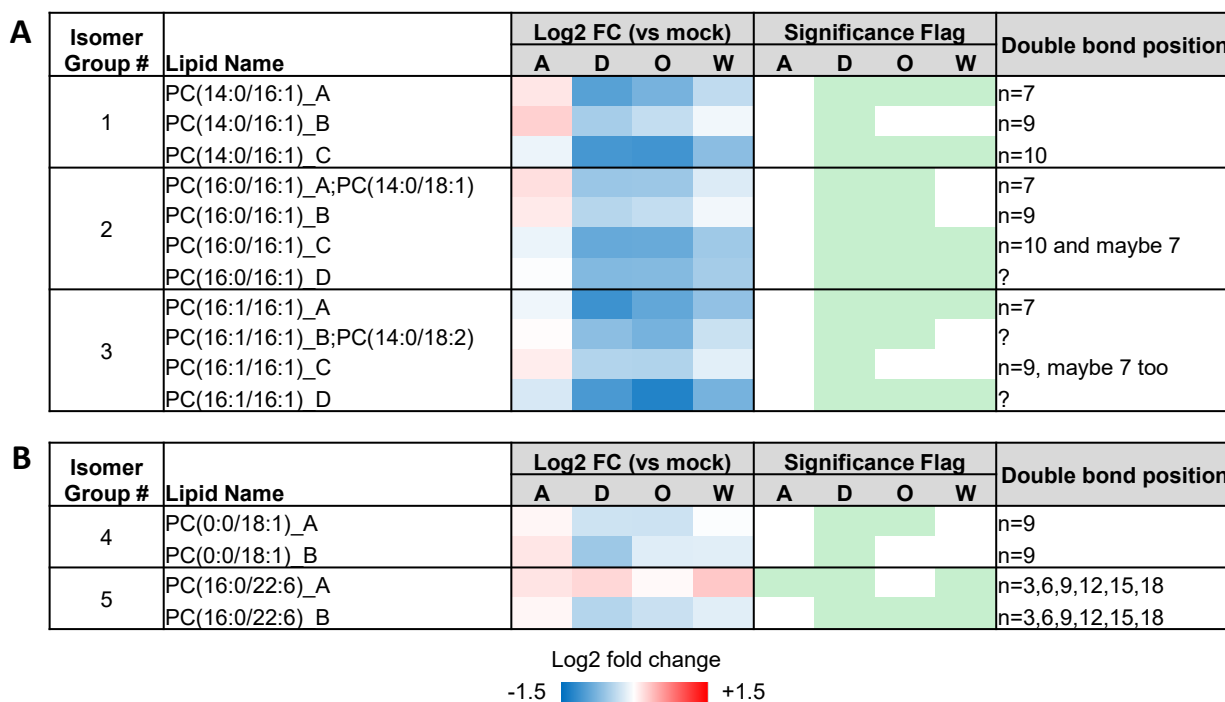


Figure 19. Assigned double bond positions to statistically significant lipids that were altered with SARS-CoV-2 variant infection of A549 cells. The statistical significance is compared to the mock-infected control.

Enrichment analysis (Clair, Reehl et al. 2019) of the significantly significant lipids (using a p-value cutoff of <0.001) that were altered during infection revealed very similar results to the HEK293T infection study in that that the lipids that were statistically increased compared to mock were enriched in lipids containing polyunsaturated fatty acids (PUFAs), in particular, phospholipids containing the fatty acid 20:4 (likely arachidonic acid), and sphingolipids with a sphinganine backbone. Also, similar to the HEK293T infection, lipids that were significantly decreased (using a p-value cutoff of <0.001) with infection were statistically enriched in monounsaturated fatty acids. A couple of unique differences between the variants included, for the lipids that statistically increased with infection, an enrichment in phosphatidylinositol was only noted in wildtype and cholesterol esters in delta and wildtype.

5.0 References

1. Andrianaivoarimanana, V., D. M. Wagner, D. N. Birdsell, B. Nikolay, F. Rakotoarimanana, L. N. Randriantseheno, A. J. Vogler, J. W. Sahl, C. M. Hall, N. Somprasong, S. Cauchemez, H. P. Schweizer, H. Razafimandimby, C. Rogier and M. Rajerison (2022). "Transmission of Antimicrobial Resistant *Yersinia pestis* During a Pneumonic Plague Outbreak." Clin Infect Dis **74**(4): 695-702.
2. Burnum-Johnson, K. E., J. E. Kyle, A. J. Einfeld, C. P. Casey, K. G. Stratton, J. F. Gonzalez, F. Habyarimana, N. M. Negretti, A. C. Sims, S. Chauhan, L. B. Thackray, P. J. Halfmann, K. B. Walters, Y. M. Kim, E. M. Zink, C. D. Nicora, K. K. Weitz, B. M. Webb-Robertson, E. S. Nakayasu, B. Ahmer, M. E. Konkel, V. Motin, R. S. Baric, M. S. Diamond, Y. Kawaoka, K. M. Waters, R. D. Smith and T. O. Metz (2017). "MPLEx: a method for simultaneous pathogen inactivation and extraction of samples for multi-omics profiling." Analyst **142**(3): 442-448.
3. Clair, G., S. Reehl, K. G. Stratton, M. E. Monroe, M. M. Tfaily, C. Ansong and J. E. Kyle (2019). "Lipid Mini-On: mining and ontology tool for enrichment analysis of lipidomic data." Bioinformatics **35**(21): 4507-4508.
4. Deatherage Kaiser, B. L., D. N. Birdsell, J. R. Hutchison, J. Thelaus, S. C. Jenson, V. Andrianaivoarimanana, M. Bystrom, K. Myrtennas, R. F. McDonough, R. D. Nottingham, J. W. Sahl, H. P. Schweizer, M. Rajerison, M. Forsman, D. S. Wunschel and D. M. Wagner (2022). "Proteomic Signatures of Antimicrobial Resistance in *Yersinia pestis* and *Francisella tularensis*." Front Med (Lausanne) **9**: 821071.
5. Farley, S. E., J. E. Kyle, H. C. Leier, L. M. Bramer, J. B. Weinstein, T. A. Bates, J. Y. Lee, T. O. Metz, C. Schultz and F. G. Tafesse (2022). "A global lipid map reveals host dependency factors conserved across SARS-CoV-2 variants." Nat Commun **13**(1): 3487.
6. Fischer, C. L., D. R. Blanchette, K. A. Brogden, D. V. Dawson, D. R. Drake, J. R. Hill and P. W. Wertz (2014). "The roles of cutaneous lipids in host defense." Biochim Biophys Acta **1841**(3): 319-322.
7. Guijas, C., C. Meana, A. M. Astudillo, M. A. Balboa and J. Balsinde (2016). "Foamy Monocytes Are Enriched in cis-7-Hexadecenoic Fatty Acid (16:1n-9), a Possible Biomarker for Early Detection of Cardiovascular Disease." Cell Chem Biol **23**(6): 689-699.
8. Harayama, T. and H. Riezman (2018). "Understanding the diversity of membrane lipid composition." Nat Rev Mol Cell Biol **19**(5): 281-296.
9. Holm, S. (1979). "A Simple Sequentially Rejective Multiple Test Procedure." Scandinavian Journal of Statistics: 65-70.
10. Jiang, X., Y. Duan, B. Zhou, Q. Guo, H. Wang, X. Hang, L. Zeng, J. Jia and H. Bi (2019). "The Cyclopropane Fatty Acid Synthase Mediates Antibiotic Resistance and Gastric Colonization of *Helicobacter pylori*." J Bacteriol **201**(20).
11. Kyle, J. E. (2021). "How lipidomics can transform our understanding of virus infections." Expert Rev Proteomics **18**(5): 329-332.
12. Kyle, J. E., K. E. Burnum-Johnson, J. P. Wendler, A. J. Einfeld, P. J. Halfmann, T. Watanabe, F. Sahr, R. D. Smith, Y. Kawaoka, K. M. Waters and T. O. Metz (2019). "Plasma lipidome reveals critical illness and recovery from human Ebola virus disease." Proc Natl Acad Sci U S A **116**(9): 3919-3928.

13. Kyle, J. E., K. L. Crowell, C. P. Casey, G. M. Fujimoto, S. Kim, S. E. Dautel, R. D. Smith, S. H. Payne and T. O. Metz (2017). "LIQUID: an-open source software for identifying lipids in LC-MS/MS-based lipidomics data." *Bioinformatics* **33**(11): 1744-1746.
14. Kyle, J. E., X. Zhang, K. K. Weitz, M. E. Monroe, Y. M. Ibrahim, R. J. Moore, J. Cha, X. Sun, E. S. Lovelace, J. Wagoner, S. J. Polyak, T. O. Metz, S. K. Dey, R. D. Smith, K. E. Burnum-Johnson and E. S. Baker (2016). "Uncovering biologically significant lipid isomers with liquid chromatography, ion mobility spectrometry and mass spectrometry." *Analyst* **141**(5): 1649-1659.
15. O'Donnell, V. B., J. Rossjohn and M. J. Wakelam (2018). "Phospholipid signaling in innate immune cells." *J Clin Invest* **128**(7): 2670-2679.
16. Pluskal, T., S. Castillo, A. Villar-Briones and M. Oresic (2010). "MZmine 2: modular framework for processing, visualizing, and analyzing mass spectrometry-based molecular profile data." *BMC Bioinformatics* **11**: 395.
17. Poad, B. L. J., X. Zheng, T. W. Mitchell, R. D. Smith, E. S. Baker and S. J. Blanksby (2018). "Online Ozonolysis Combined with Ion Mobility-Mass Spectrometry Provides a New Platform for Lipid Isomer Analyses." *Anal Chem* **90**(2): 1292-1300.
18. Poger, D. and A. E. Mark (2015). "A ring to rule them all: the effect of cyclopropane Fatty acids on the fluidity of lipid bilayers." *J Phys Chem B* **119**(17): 5487-5495.
19. Tsugawa, H., K. Ikeda, M. Takahashi, A. Satoh, Y. Mori, H. Uchino, N. Okahashi, Y. Yamada, I. Tada, P. Bonini, Y. Higashi, Y. Okazaki, Z. Zhou, Z. J. Zhu, J. Koelmel, T. Cajka, O. Fiehn, K. Saito, M. Arita and M. Arita (2020). "A lipidome atlas in MS-DIAL 4." *Nat Biotechnol* **38**(10): 1159-1163.

Pacific Northwest National Laboratory

902 Battelle Boulevard
P.O. Box 999
Richland, WA 99354

1-888-375-PNNL (7665)

www.pnnl.gov